EXTENSION OF BUSEMANN BIPLANE THEORY TO THREE DIMENSIONAL WING FUSELAGE CONFIGURATIONS

Kisa Matsushima*, Daigo Maruyama, Kazuhiro Kusunose***, Ryota Noguchi[$]**
***University of Toyama, Gofuku Toyama 930-8555 JAPAN, kisam@eng.u-toyama.ac.c**
**** ONERA, Meudon FRANCE, formerly Tohoku University, ***JAXA, Tokyo JAPAN,**
[$] Toyata Industries Corporation, Aichi, JAPAN, formerly Tohoku University.

Keywords: *Supersonic Busemann biplane, Three-dimensional effect, Fuselage effect, CFD*

Abstract

Busemann biplane concept is studied and extended to three dimensional configurations as well as to wing-fuselage ones using CFD techniques. Aerodynamics attributed to three dimensional biplane are computationally analyzed and discussed. For the one of three dimensional effects which could promote aerodynamic performance for biplane wing is generalized from the theoretical point of view using supersonic flow physics. In addition, the study of the aerodynamic center for the biplane is conducted.

1 Introduction

In supersonic flight, high fuel-efficiency and the reduction of sonic boom at cruising are crucial issues. Both phenomena originate in strong shock waves peculiar to supersonic flight. A biplane which was proposed by A. Busemann in 1935 could be a breakthrough in eliminating shockwaves [1,2]. One of the authors, K. Kusunose started the research of the biplane aiming the practical use of it at Tohoku University in 2004. After that the research has made fruitful progress [3-12].

In this article, Busemann biplane concept is studied and extended to three dimensional (3D) configurations as well as to wing-fuselage ones using CFD techniques. Selected topics which seem characteristic to the biplane including the aerodynamic center are analyzed in detail to construct simple models of flows about biplanes. All the simulations here are conducted by a unstructured mesh CFD solver called TAS-FLOW developed in Nakahashi laboratory of Tohoku University [13].

3 Bsumann Biplane Theory and Its CFD Reproduction

2.1 Original Concept

The original idea was in the presentation by Busemann on the 5th Volta Congress more than 70 years ago. Figure 1 shows what is called Busemann biplane. It is the combination of two triangle elements, Δabc and Δdef. When the Busemann biplane is on a supersonic flowfield, Shock waves which emanate from a and c are cancelled out with expansion waves from e,

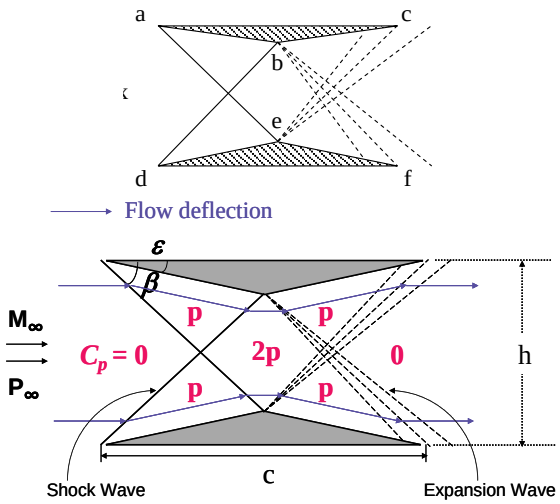

Fig. 1 Busemann Biplane.

and shockwaves from d and f are cancelled out with expansion waves from b. The lower diagram of Fig. 1 explains the Cp situation predicted by the linear theory inside of the two elements. It indicates that all the Cp values along a-b, b-c, d-e, and e-f are identical, which does yield zero drag. One problem of the concept is that the gap 'h' between the two elements should alter with the variation of Mach number 'M_∞'or the wedge angle 'ε'.

2.1 CFD Analysis Results and Discussion

Two dimensional (2-D) CFD calculation is conducted on a Busemann biplane using Euler equations with M_∞ of 1.7. In that case, each element of the biplane was an isosceles triangle whose base was 1.0 and height is 0.05. The gap is set 0.5. The calculated Cp distribution around each triangle element is plotted by red symbols in Fig.2. There Cps by Busemann's theory are also shown by a blue line. Both of Cps agree

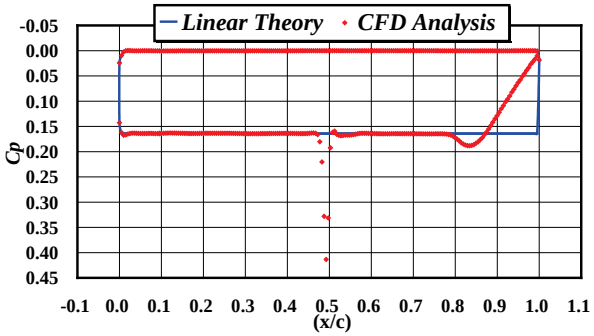

Fig. 2 Cp on Each Element by CFD and Linear Theory

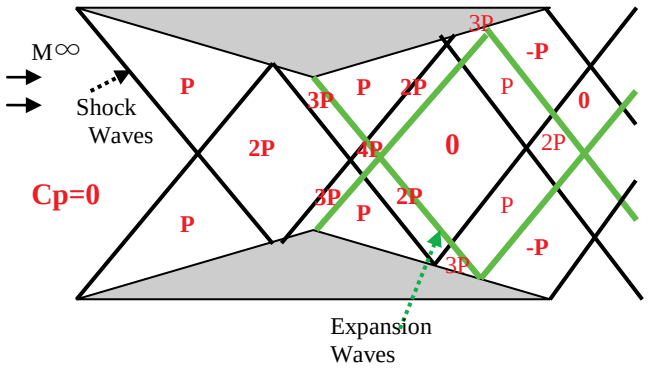

Fig. 3 Explanation for Pressure Peak by Inappropriate Layout of Two Elements.

except those near the trailing edge. The difference there comes from the nonlinear propagation of expansion waves emanating from the mid-chord apex. This implies the biplane actually has some amount of drag force, of cause it is not much. Cp values of 'p' along surface a-b and d-e can be calculated by the oblique shock relation, Eq. (1) [2]. β is the wedge angle of b-a-c or f-d-e in radian and is supposed to be quite small. Variation in Cp by deflection of flow angle is

$$Cp = c_1\varepsilon + c_2\varepsilon^2 \qquad (1)$$

where

$$c_1 = \frac{2}{\sqrt{M_\infty{}^2 - 1}}\ ,\quad c_2 = \frac{(M_\infty{}^2-2)^2 + \gamma\, M_\infty{}^4}{2(M_\infty{}^2-1)^2} \qquad (2)$$

Here, ε is arctan(0.1)=0.0997(rad) and M_∞=1.7. Therefore, 'p' in Fig.1 is 0.164 which agrees well with CFD Euler analysis in Fig. 2.

In Fig.2, a sharp pressure peak is observed in Cp distribution around *x/c*=0.5 of the CFD results. The existence of such peak indicates that the cancellation effect of shock waves and expansion waves is not sufficient. Figure 3 explains the insufficient cancellation. In Fig.3, when flows pass across shock waves (solid line), Cp increases by "p", while they do expansion waves (dashed lines), Cp decreases by "2p". The peak is caused by the fact that the shock waves from the leading edges hit the inner surfaces a little bit ahead the mid-chord apex. It yields to three times of "p" high pressure region on the surface of each element. In fact, the peak Cp in Fig. 2 is about three times of "p" that is 0.163x3=0.489.

To realize better layout of two elements as well as the better geometry of each element, non linearity of wave interaction and propagation should be considered. Thus, we conducted design of biplane airfoil based on nonlinear flow equations. Finally, the biplane airfoil geometry is obtained which realized lower drag than any existing one [4,5,7].

3 Extension to Three Dimensional Biplane

3.1 Parametric Study for Planform

The 2-D biplane is extended to a wing. After the computational study of a lot of different planforms, the best configuration has been determined. The configuration is presented in Fig. 4 with mesh visualizations of the wing and Cp distribution color map at the cruise Mach number of 1.7. For the study the section airfoil geometry at all span stations was unique, which is almost the same as we used in the section 2. The gap between the two elements is set 0.505 not 0.500. The reference area is 1 and the taper ratio is 0.25. The semi-span length and the aspect ratio are 1.6 and 5.12, respectively. Using the planform, we have conducted parametric study to find the best sweep angle [11]. The L/D of the wings is as almost same as that of two dimensional configuration. This fact which is a pleasant surprise, depends on favorable three dimensional (3-D) effects, while usually wing L/D becomes lower because of 3-D effects compared with that of the section airfoils. Thus, to investigate the 3-D effect associated with biplane wings, we compare the best biplane wing (case2) with another one of a different sweep angle (case1)[11,12]. In Fig. 5 span-wise Cd, and in Fig. 6 inner surface Cp distributions, and chord-wise Cp at a span station are compared. In span-wise Cp, case2 realize lower section Cd than 2-D case from the 0.4 to 0.8 semi-span stations. Lower Cd is caused by the higher Cp on the trailing portion (bc and ef edges of Fig.1) at the span station. This is one of the 3-D effects which we will analyze in the followings.

3.1 Analysis using Supersonic Aerodynamics

At first compression at the leading edge is estimated using the independent theory of awept wings. Here, the wing section in Fig. 6 is considered. Figure 7 is overall view while flow situations around the lower element are shown in Fig. 8. Effective Mach number for case 1 and 2 are M_∞ and $M_\infty \cos\theta_2$, respectively. Then, effective wedge angles for case1 is ε and that for case2 is $\varepsilon 2$ which relates ε as $\tan\varepsilon 2 = \tan\varepsilon / \cos\theta_2$. If ε and $\varepsilon 2$ are small, the relation can approximate to $\varepsilon 2 = \varepsilon / \cos\theta_2$. They are substituted Eq.(1) and (2) to obtain Cp values on the wind side of element. M_∞ is 1.7, ε is 0.0997 and θ_2 is 0.234 in radian. For case1, the Cp value is 0.164 same as that for 2D flows. For case 2, the Cp is 0.168

Next, M_{1f} and M_{2f} should be obtained using the following oblique shock equations, Eq.(3) and(4) [2].

$$\tan\beta = 2\cot\beta \frac{M_\infty \sin\beta - 1}{M_\infty(\gamma + \cos 2\beta) + 2} \qquad (3)$$

$$M_{1f} = \frac{1}{\sin(\beta - \varepsilon)} \sqrt{\frac{1 + \{(\gamma-1)/2\} M_\infty^2 \sin^2\beta}{\gamma M_\infty \sin^2\beta - (\gamma-1)/2}} \qquad (4)$$

M_∞ and ε are replaced by $M_\infty \cos\theta_2$ and $\varepsilon/\cos\theta_2$, respectively to obtain M_{2f}. Then, conducting the similar calculation for second compression process, Cp after the second compression, and M_1 and M_2 are determined. Actually, the Cp vales 0.343 and 0.378 for case 1 and 2 respectively. M_1 is 1.30 and M_2 is 1.32. When the effective Mach number for expansion at the mid-chord apex is calculated for 3D, velocity

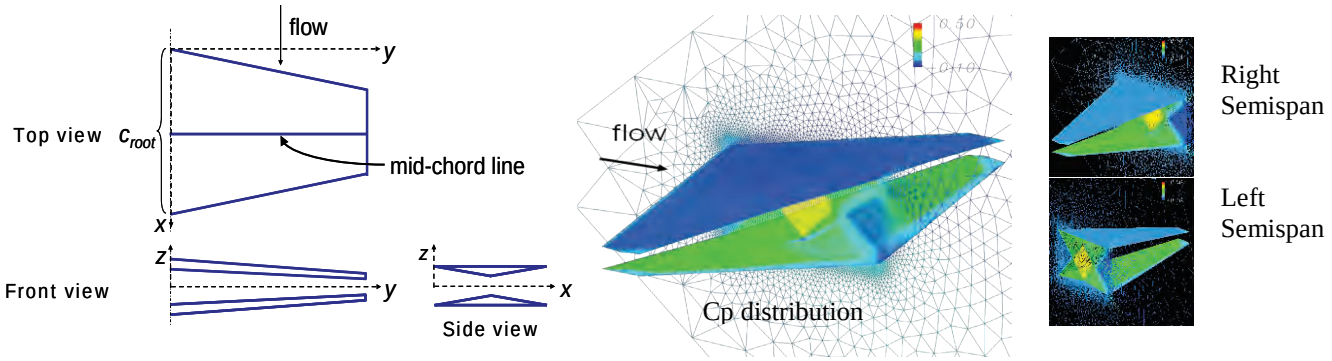

Fig.4 Extension of Busemann biplane to wing configurations and its flow analysis. (Mach 1.7, AOA=0deg.)

property parallel to the swept leading edge should be taken account of and the effective Mach number yield to $\sqrt{M_2^2 + M_\infty^2 \sin^2\theta_2}$ for case2. Finally, we can obtain Cp values on the lee side surface of inner surface of the biplane wings by calculating Eqs.(1) and (2). For 2D, M_1 and -ε are used as M_∞ and ε in those Eqs. For case1, $M_1 \cos\theta_1$ and $-\varepsilon_1 = -\varepsilon\cos\theta_1$, where is 0.234 and For case2, $\sqrt{M_2^2 + M_\infty^2 \sin^2\theta_2}$ and $-\varepsilon$ are used. The obtained Cp value for each case is as follows; 0.166 for 2D, 0.158 for case1 and 0.172 for case2. Thus, using the simple flow-field model illustrated in Figs.7 and 8, the 3D effect associated with sweep angles of leading and trailing edges is resolved.

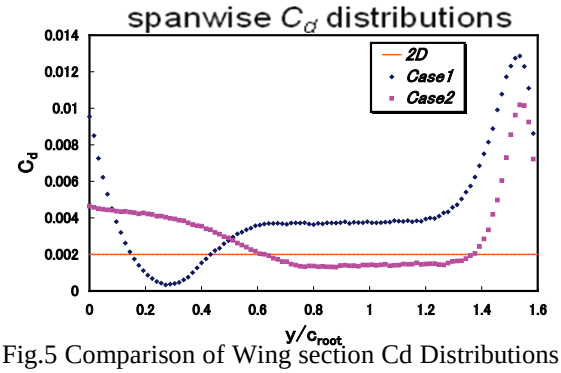

Fig.5 Comparison of Wing section Cd Distributions along the Spanwise Direction with Cd of pure 2D (solid lines).

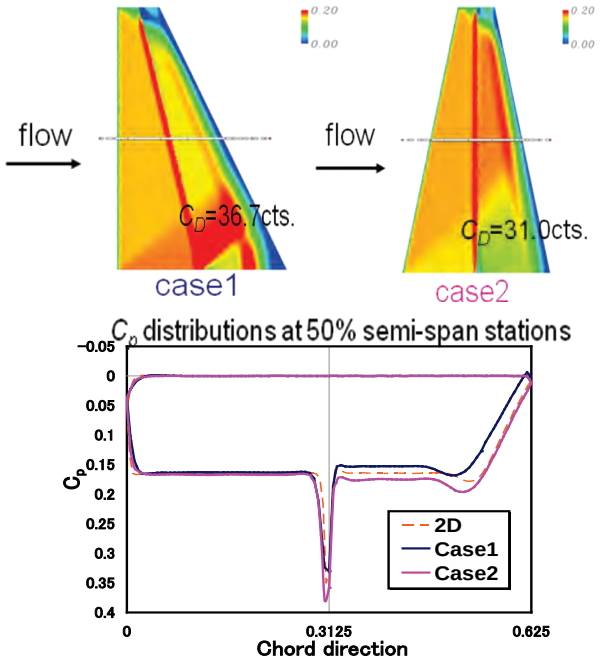

Fig.6 Comparison of the Wing Configuration of Good Performance (Case2) with Another One of Less Performance (Case1).

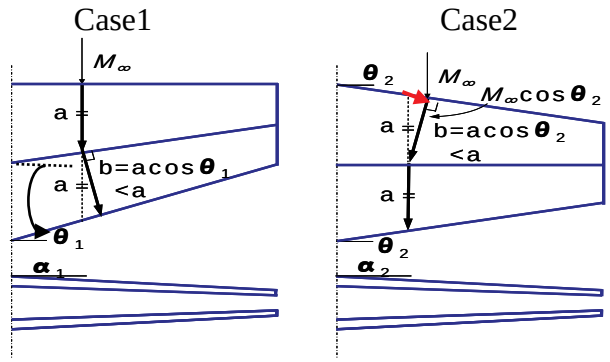

Fig. 7 Overview of Effective Flow streams normal to Edge.
(Top and Front Views of Two Tapered Biplane Wings)

Lower Elements of Biplane Wing of Case1 and Case2.

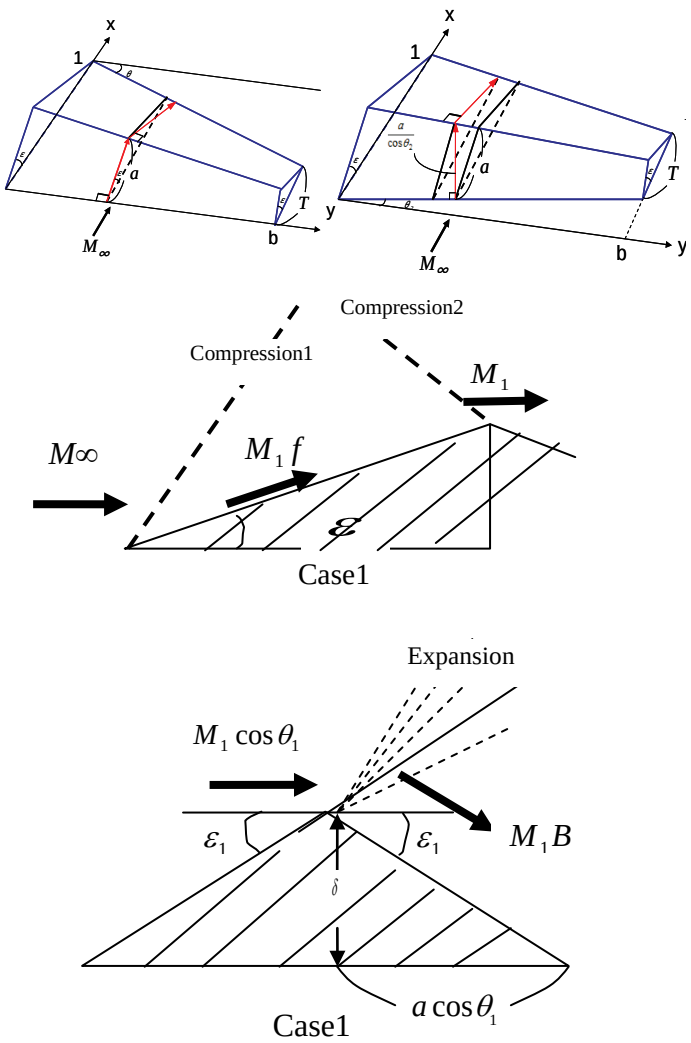

Fig. 8 Supersonic Flow Model abo ut Biplane Wings in Three-dimension Based on Two-dimensional Theory.

4 Biplane Wing-Fuselage Combination

4.1 Wing-Fuselage Configuration

Figure 9 shows a wing-fuselage configuration. The fuselage has been proposed by Ref.[10] which generates strong shock waves and expansion waves. The fuselage has conical configuration at the tip and a rectangular parallelepiped at the back. The purpose of the wing-fuselage simulation is just to investigate how badly the fuselage affects the good biplane wing aerodynamic performance. The body shape is chosen in order to generate strong shock waves and expansion waves from the body. The wing is attached there so that disturbances from the body can influence the entire wing. A baseline wing configuration used in the study is a Busemann biplane wing with the tapered planform.

Two types of biplane wings are used for the wing-fuselage configurations. Both types are identical except for the existence of winglet. The wing has the section shape of a Busemann biplane airfoil whose total thickness-chord ratio is 0.10 and its gap-to-chord ratio between two elements has been adjusted for a cruise speed of Mach 1.7 to be 0.505.

Fig. 9 Extension of Busemann Biplane to wing-fuselage configurations.

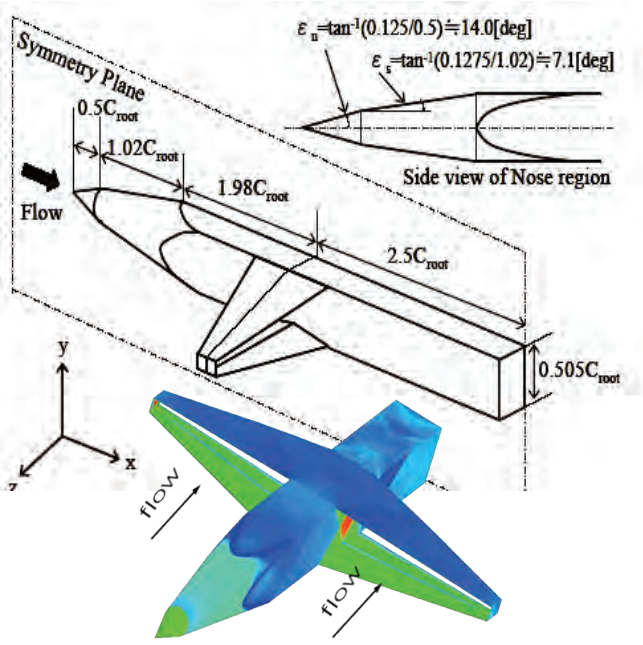

The wing has the tapered planform discussed in the previous section; with the taper ratio being 0.25. As shown in Fig. 10, there are four configurations each of which has different wing location along the x direction (Xw) from each other. Therefore, we simulate eight types of wing-body configurations four without winglet (w/o wlt) and four with winglet (w/ wlt) [9,10,12].

4.2 Aerodynamic performance at the Cruise Condition

Several wing-body configurations are simulated in order to investigate influence by the existence of fuselage on supersonic biplane wings. Inviscid flow analyses have been conducted using TAS code with 2.0 million grid point of an unstructure mesh[13].

Figure 10 shows surface C_p distributions at zero lift conditions (zero angle of attack) of the wing-body configurations w/o wlt. Those C_p distributions are on the inner surfaces of the biplane wings as well as fuselage. For the cases of x_w=4 and 4.5, wings are affected by the expansion waves only, On the other hand, there are noticeable differences when x_w=3 and 3.5, in which wings are affected by not only the expansion waves but also the compression waves. Areas near the wingtip having high pressures regions are effect of shock wave from the fuselage nose. From the view point of stability for flight control, it is undesirable.

Figure 11 shows drag-polar curves of the wings of the wing-fuselage configurations (w/o wlt and w/ wlt) comparing that of the wing alone (simple wing) case. All the wing-body configuration cases except the case of x_w=3 have better aerodynamic performance than the wing alone cases. In a summary, on both w/o wlt and w/ wlt, the areas affected by the compression waves will have higher wave drag than that of isolated wing cases except for the case when the reflection of the compression waves from the winglet exists. On the other hand, the areas affected by the expansion waves have better aerodynamic performance in all cases. The biplane wing is reasonably robust against the disturbances generated by the fuselage [9, 10].

Moreover, aerodynamic characteristics of the biplane wing of the wing-body configuration can be improved compared with that of the isolated wing case [12].

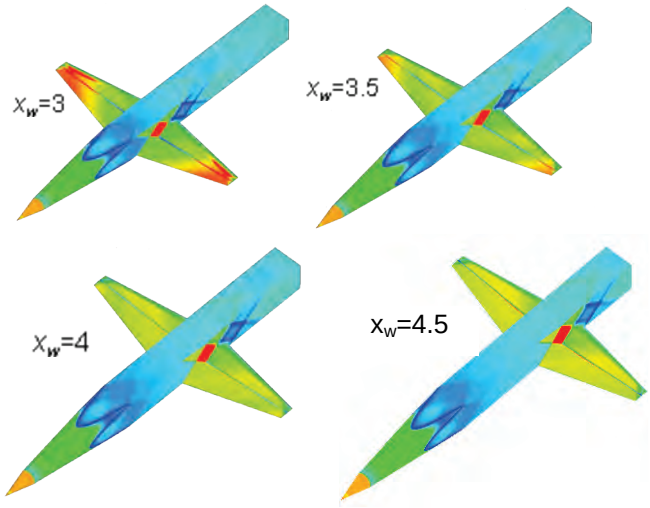

Fig. 10 Comparison of Surface Cp Distributions in the Inner Side of a Biplane (upper surface of the lower wing). (Mach 1.7, AOA=0deg.)

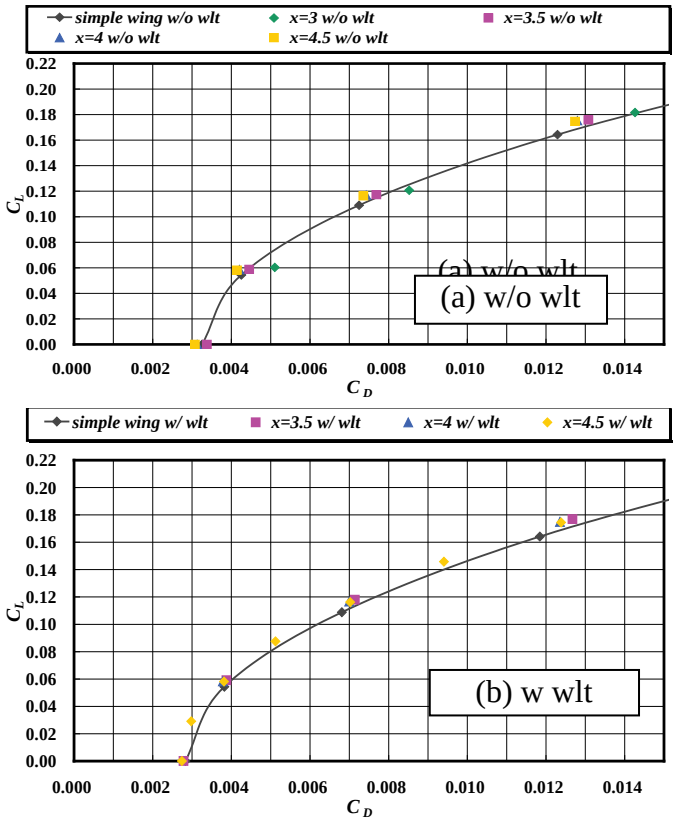

Fig. 11 Drag-polar Curves of Bipane Wings affected by Fuselage.

5 Preliminary Examination on Aerodynamic Center (A.C)

5.1 Problems Concerning A.C.

Some issues concerning with the movement of the aerodynamic center (A.C.) of wings should be solved for practical supersonic flight. When considering a monoplane wing, its A.C. is at the 25% chord in a subsonic flight (i.e. $M_\infty < 1.0$) whereas it is at the 50% chord in a supersonic flight (i.e. $M_\infty > 1.0$). Therefore, the trim control of the supersonic airplanes becomes complex and difficult. In fact, for Concorde, they equipped eleven fuel tanks so that they could transfer fuel from a tank to another one. The fuel moved its location in order to accommodate with the change of the A.C. location. Thus, the change of the A.C. location of a biplane should be investigated for a wide range of its flight speed. In this section, two-dimensional analysis will be discussed [14**].**

5.2 Biplane and Diamond Airfoils

In order to compare the biplane's A.C. with the monoplane's one, both of the Busemann-type biplane and the diamond airfoil were numerically analyzed. Figure 12 shows the both airfoils and the coordinate axes to define A.C. location. The chord length is 1.0. The leading and trailing edge positions are 0.0 and 1.0, respectively. The biplane examined here is the one used in the previous section as the wing section airfoil.

CFD flow simulations were conducted to obtain lift and pitching moment coefficients for the 27 cases for each of both airfoils. The 27 cases contain a subsonic range from 0.2 to 0.6 and a supersonic range from 1.7 to 2.0 of the Mach number and 0, 1 and 2 degrees of the angle of attack. To determine the A.C. location, we assumed that the A.C. would be located along the ***x***-axis in Fig. 12. From the study, it was found that. the A.C. of biplanes stayed at 25 - 27% chord both in subsonic and supersonic cases. On the other hand, the A.C. location of diamond airfoils was 28% chord for the flow speed of Mach 0.2 - 0.6, and it was 44 - 45% chord for Mach 1.7 - 2.0 [14].

5.3 Biplane and Diamond Airfoils

The further investigation was conducted to consider the primary factor to determine the A.C. location. The load distributions along a chord axis were investigated. The surface Cp distributions as well as load distributions are displayed with the airfoil geometry in Figs. 13-16. Figure 13 includes the simulation results of the diamond airfoil at the speed of M_∞=0.5. The case of the biplane airfoil at the speed of M_∞=0.5 is in Fig. 14. The case of the diamond airfoil at the speed of M_∞=1.7 is in Fig. 15. And the case of the biplane airfoil at the speed of M_∞=1.7 in Fig. 16. Each case has two different Cp distributions for the angle of attack of 0 degree (deg.) and 2 degs., respectively. In Figs. 13 and 15 of diamond airfoil cases, the pink lines indicate the upper-surface Cps while the blue ones do the lower surface Cps. In Figs.14 and 16 of biplane cases, the pink lines indicate the upper-element Cps while the blue ones do the lower element Cps. From the biplane cases, it can be seen that, in subsonic flows, the lower element generates lift whereas the upper one does negative lift, on the other hand, in supersonic flows, the upper element generates lift whereas the lower one does negative.

Next, load distributions along the chord are studied. Integrating the Cp distributions, the load distribution graphs are produced in Figs. 13-16. Each case consists of load distributions along chord when the angle of attack is 1.0 deg. and 2.0 degs. When 0 deg, the load is zero all over the airfoil. Observing the load variations, in case in Fig.15, the rear half of the airfoil generates some lift, which yields to set the A.C. location around 50% chord. However, in the other cases, the rear half of the airfoil do not generate lift, yielding the A.C. location around 25% chord. The A.C. of Busemann-type biplanes designed for M_∞=1.7 stays almost same location, 25% chord, both in subsonic flows of M_∞ from 0.2 to 0,6, and in supersonic flows of M_∞ from 1.7 to 2.0.

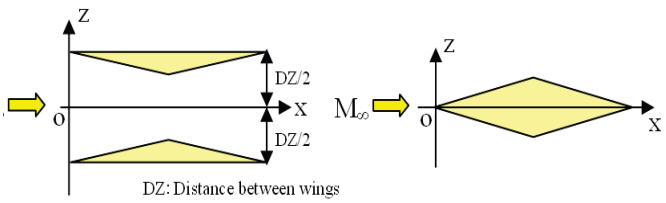

Fig. 12 Biplane and Diamond Airfoils.

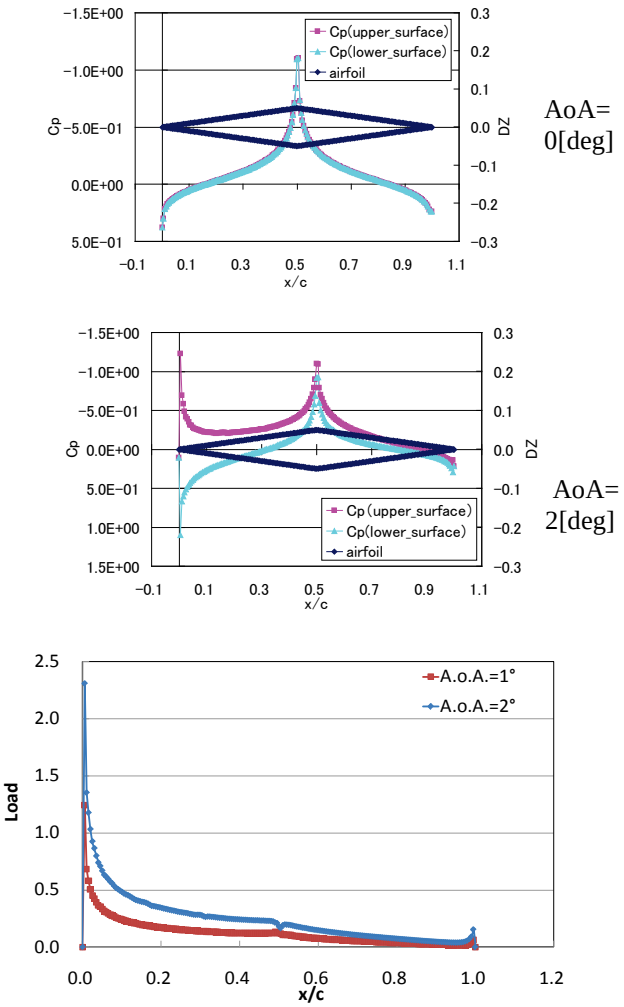

Fig. 13 Surface Cp and Load Distribution on the Diamond Airfoil at Mach 0.5 and AoA of 0, 1, and 2 degree(s).

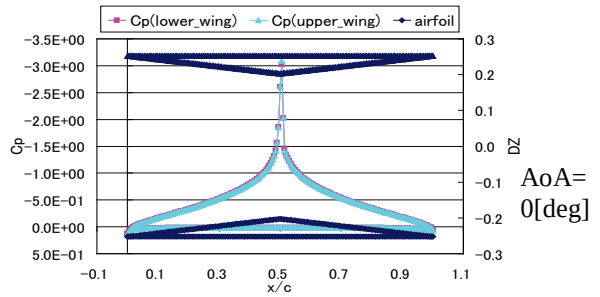

AoA= 0[deg]

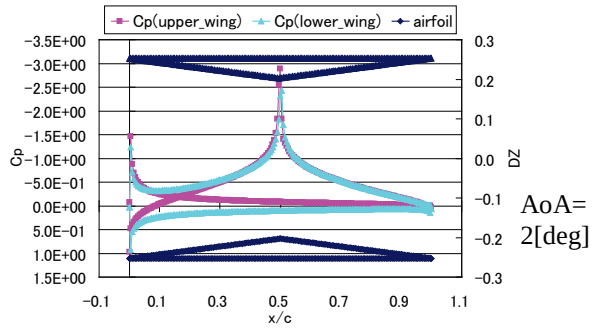

AoA= 2[deg]

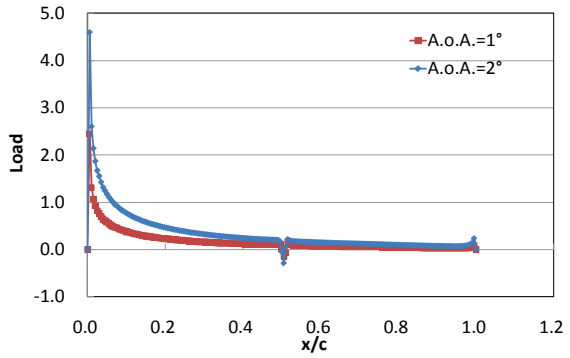

Fig. 14 Surface Cp and Load Distribution on the Biplane Airfoil at Mach 0.5 and AoA of 0, 1, and 2 degree(s).

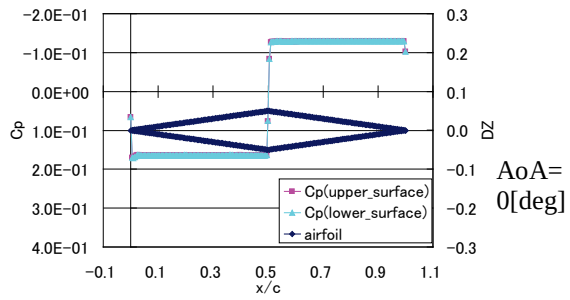

AoA= 0[deg]

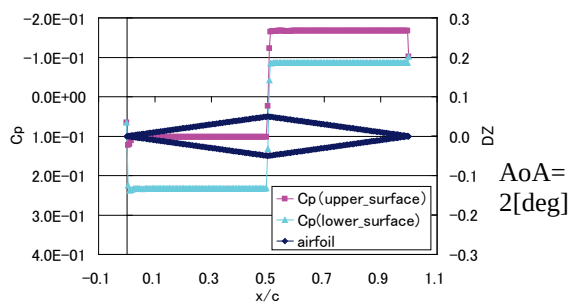

AoA= 2[deg]

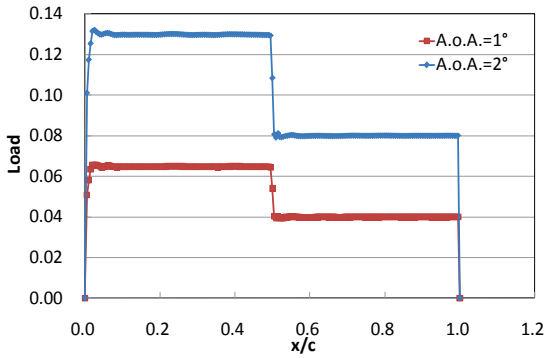

Fig. 15 Surface Cp and Load Distribution on the Diamond Airfoil at Mach 1.7 and AoA of 0, 1, and 2 degree(s).

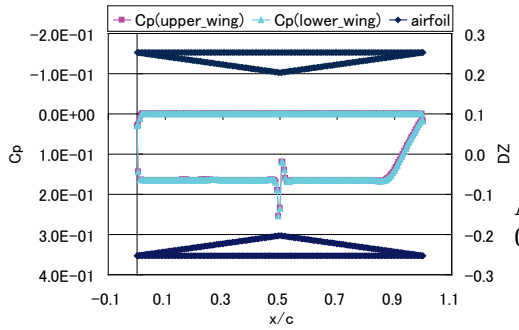

AoA= 0[deg]

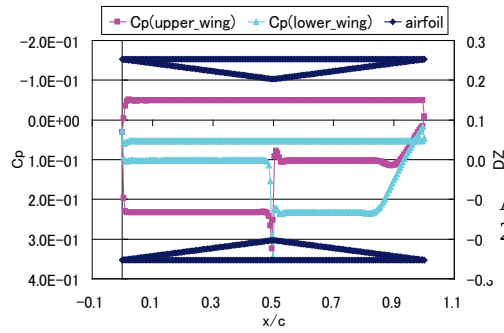

AoA= 2[deg]

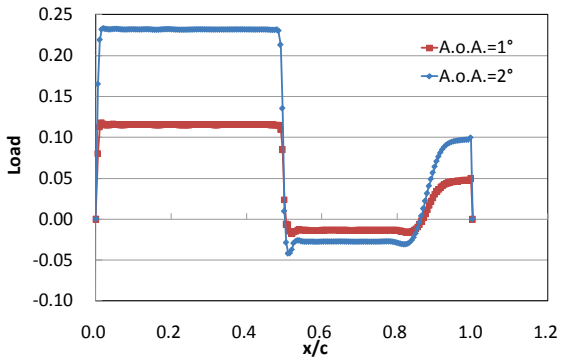

Fig. 16 Surface Cp and Load Distribution on the Biplane Airfoil at Mach 1.7 and AoA of 0, 1, and 2 degree(s).

6 Conclusions

Three subject concerning to making the practical use of a biplane concept were computationally analyzed and discussed. The biplane concept was based on the idea in 2D flows by Adolf Busemann in 1930s.

The first subject is to extend the 2-D biplane to 3-D biplane wings, a study was attempted. In this study the tapered-wing planform with taper ratio of 0.25 and aspect ratio of 5.12 was selected [11,12]. The 2-D biplane configuration was used as wing-section geometry of the tapered wing. We paid attention to favorable 3D effects that improved L/D performance of 2D biplane cases. Among the CFD results when studying sweep angle effect, one of phenomena of favorable 3D effects was found. With a certain sweep angle of the wing, the section Cd value was lower than that of 2D case, around 20% to 80% semi span-station. It was resulted from the special Cp distribution profile on the section at those span-stations. We constructed a mathematical model using the supersonic flow theories by Busemann, Prandtl and Meyer and analyzed the phenomena. The model was simple, but worked well to resolve the 3D effect.

As the second subject, wing-fuselage configurations were simulated to investigate wave-interference effects of the fuselage on the tapered biplane wings [9,10,12]. In the study a fuselage geometry which generates strong shock waves and expansion waves at its nose region was selected to investigate the sensitivity of the biplane wing to the non-uniform upstream flows. Parametric studies on the interference effects between body and supersonic biplane wings were performed using several differrent wing locations to the body. In general, supersonic biplane wings perform better when they are exposed by expansion waves [12]. For wing-fuselage configurations, when biplane wings are located in expansion-wave regions biplane wings perform better than the isolated wing configurations.

The third subject is the consideration of the location of A.C. This was done in 2D simulation. Simulations on subsonic and supersonic flows were conducted about the biplane as well as a diamond airfoil which stood for monoplanes [14]. In subsonic flows, the A.C.. location of the airfoil was around 25% chord whereas in supersonic, it was around 50%. On the other hand, the A.C. of Busemann-type biplanes designed for M_∞=1.7 stayed almost same location, 25% chord, both in subsonic and in supersonic flows. The reason why the A.C. of the biplane stayed same location was also analyzed.

References

[1] Busemann, A., Aerodynamic Lift at Supersonic Speeds , *Proceeding. Volta Congress*, pp.315-347, Italy, 1935.

[2] Liepmann, H. W., and Roshko, A., *Elements of Gas Dynamics*, John Wiley & Sons, Inc., New York, 1957.

[3] Kusunose, K., Matsushima, K., Goto, Y., M., Maruyama, D., Yamashita, H. and Yonezawa, M., A Study in the Supersonic Biplane utilizing its Shock Wave Cancellation Effect, *Journal of The Japan Society for Aeronautical and Space Sciences*, Vol. 55, No. 636 , pp.1-7, 2007 [In Japanese].

[4] Matsushima, K., Kusunose, K., Maruyama, D., Matsuzawa, T., Numerical design and assessment of a biplane as future supersonic transport, *Proceedings 25th ICAS Congress*, ICAS 2006-3.7.1, Hamburg Germany, September, 2006.

[5] Matsushima, K. Maruyama, D., Matsuzawa, T., Numerical modeling for Supersonic Flow Analysis and Inverse Design, *Proceedings of Lectures and Workshop International –Recent Advances in Multidiciplinary Technology and Modeling-*, JAXA-SP-07-008E, pp. 185-194, Tokyo Japan, May 2008.

[6] Yamashita, H., Obayashi, S. and Kusunose, K., Reduction of Drag Penalty by means of Plain Flaps in Boomless Busemann Biplane. *International Journal of Emerging Multidisciplinary Fluid Sciences*, Vol. 1, No. 2, pp.141-164, 2009.

[7] Maruyama, D., Kusunose, K. and Matsushima, K., Aerodynamic characteristics of a two-dimensional supersonic biplane, covering its take-off to cruise conditions, *International Journal of Shock Waves*, Vol. 18, No. 6, pp.437-450, 2009.

[8] Yonezawa, M. and Obayashi, S., Reducing Drag Penalty in the Three-dimensional Supersonic Biplane, *Journal of Aerospace Engineering*, Vol. 223, No. 7, pp.891-899, 2009.

[9] Odaka, Y., and Kusunose, K., Interference Effect of Body on Supersonic Biplane Wings, *40th Fluid Dynamics Conference and Aerospace Numerical Simulation Symposium 2008*, Paper 1B10, June 2008 [In Japanese].

[10] Odaka, Y., and Kusunose, K., A Fundamental Study for Aerodynamic Characteristics of Supersonic Biplane Wing and Wing-Body Configurations, *Journal of The Japan Society for Aeronautical and Space Sciences*, Vol. 57, No. 664, pp.217-224, 2009. (in Japanese).

[11] Maruyama, D., Matsushima, K., Kusunose, K. and Nakahashi, K., Three-Dimensional Aerodynamic Design of Low Wave-Drag Supersonic Biplane Using Inverse Problem Method, *Journal of Aircraft*, Vol. 46, No. 6, pp.1906-1918, 2009.

[12] Maruyama, D., Nakahashi, K., Kusunose, K. and Matsushima, K., Aerodynamic Design of Supersonic Biplane –Toward Efficient Supersonic Transport -, *CEAS 2009, European Air and Space Conference*, Manchester, UK, 2009.

[13] Nakahashi, K., Ito, Y., and Togashi, F., Some Challenge of Realistic Flow Simulations by Unstructured Grid CFD, *International Journal for Numerical Methods in Fluids*, Vol. 43, pp.769-783, 2003.

[14] Noguchi, R., Maruyama, D., Matsushima, K., Nakahashi, K., Study of the Aerodynamic center and Aerodynamic Characteristics of Supersonic Biplanes in a wide Mach Number Range, Proceedings of the 22nd CFD symposium by Japan Society of Fluid Mechanics, B6-1, pp. 1-7, Tokyo, Japan, December, 2008 [In Japanese].

Contact Author Email Address

kisam@eng.u-toyama.ac.jp

Copyright Statement